Research Article

Received: 3 June 2020 Revised: 28 December 2020 Accepted article published: 13 January 2021 Published online in Wiley Online Library: 2 February 2021

(wileyonlinelibrary.com) DOI 10.1002/pi.6189

High-performance hybrid luminescent-scattering solar concentrators based on a luminescent conjugated polymer

Yilin Li,[a*] Yujian Sun,[b] Yongcao Zhang,[c] Yuxin Li[d] and Rafael Verduzco[a*]

Abstract

Luminescent solar concentrators (LSCs) are considered a promising building-integrated photovoltaic technology. Over the past decade, numerous luminophores have been developed for LSCs. However, conjugated polymers are rarely reported for LSCs despite their wide application in other fields. In this study, we investigated a luminescent conjugated polymer, poly(naphthalene-*alt*-vinylene) (PNV), for LSCs. PNV exhibits an absorption wavelength (λ_{abs}) of 535 nm, an emission wavelength (λ_{em}) of 632 nm and a photoluminescence quantum yield of 0.40 in a poly(methyl methacrylate) matrix. When tested under outdoor direct sunlight (1000 W m^{-2} ± 10%) and indoor diffuse light-emitting diode (LED) light (10 W m^{-2} ± 10%), the PNV-based LSCs with a size of 12 in. (30.48 cm) exhibited power conversion efficiencies (η_{LSC}) of up to 2.9% and 3.6%, respectively, and concentration ratios (*C*) of up to 1.49 and 3.53, respectively. The external quantum efficiencies of the LSCs and the edge emission spectra of the luminescent waveguides were analyzed to reveal the impact of surface scattering treatment on device performance. Monte Carlo ray-tracing simulation was employed to project the performance of large-area LSCs with sizes of up to 120 in. (304.8 cm). For the LSCs under outdoor direct sunlight and indoor diffuse LED light, the projected η_{LSC} values were 1.29% and 0.88%, respectively, and the projected *C* values were 6.73 and 8.62, respectively. This study suggests that high-performance LSCs can be achieved through luminescent conjugated polymers.

Supporting information may be found in the online version of this article.

Keywords: luminescent solar concentrator; conjugated polymer; power conversion efficiency; concentration ratio; surface scattering treatment; Monte Carlo ray-tracing simulation

INTRODUCTION

Building-integrated photovoltaic (BIPV) technologies offer attractive and promising solutions for electricity production from a renewable source in the urban environment, where the energy demand cannot be directly met by rooftop solar panels due to the requirement of high power consumption density.[1–5] Among several types of BIPV technologies, luminescent solar concentrator (LSC) technology is one of the most extensively studied as it provides a feasible solution to seamlessly integrate photovoltaic (PV) devices with buildings, meanwhile delivering visual comfort for human beings.[6–11] A conceptual picture of the BIPV-based LSCs is shown in Fig. 1(a), where a house is designed with colorful LSCs as French windows. A typical LSC consists of a planar waveguide doped with luminophores and solar cells attached to the edges, which is depicted in Fig. 1(b). A fraction of sunlight enters the luminescent waveguide. Typically, short-wavelength solar photons are absorbed by the luminophores and converted to long-wavelength photons inside the waveguide, which are transported to the edges through total internal reflection (TIR) and absorbed by the solar cells. With this design, the luminescent waveguide concentrates the sunlight from a large area to a small area, reducing the material use of solar cells. Beyond a critical size of the waveguide, the solar cells output a higher power than they do when facing direct sunlight, which makes LSCs cost-effective.[12–14] Additionally, studies have shown that LSCs can perform optimally under different light conditions, especially the indoor environment.[15,16]

Although the concept of LSCs was introduced in the 1970s,[17,18] research activities on LSCs have been more vigorous in recent decades, primarily due to the significant advancement of the research on luminophores. Over the past decade, numerous luminophores have been developed. They are typically categorized as organic dyes[19–21] (e.g. those based on aggregation-induced emission[22–24]), quantum dots,[25–28] rare-earth complexes[29–32] and

* *Correspondence to: Y Li or R Verduzco, Department of Chemical and Biomolecular Engineering, Rice University, Houston, TX 77005, USA. E-mail: yilinli@rice.edu (Li); E-mail: rafaelv@rice.edu (Verduzco)*

a *Department of Chemical and Biomolecular Engineering, Rice University, Houston, TX, USA*

b *School of Environmental and Forest Sciences, University of Washington, Seattle, WA, USA*

c *Department of Mechanical Engineering, University of Houston, Houston, TX, USA*

d *Department of Chemistry, University of Cincinnati, Cincinnati, OH, USA*

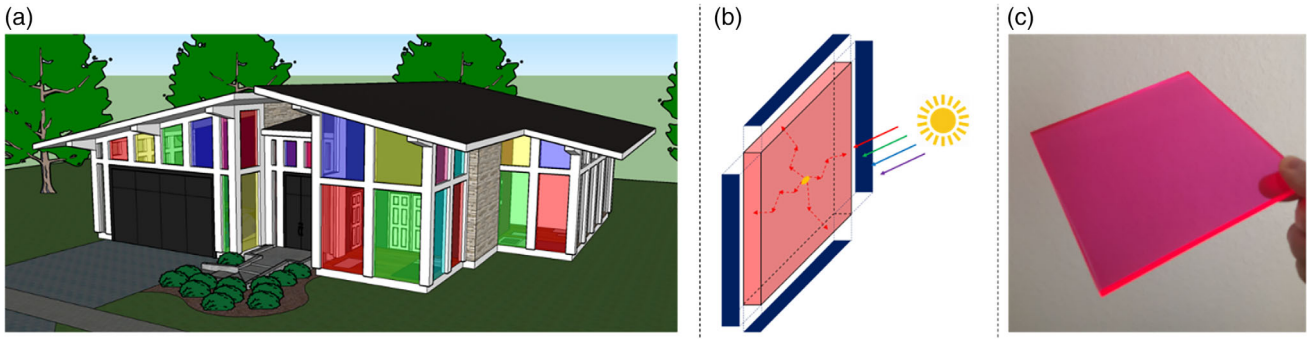

Figure 1. (a) A conceptual picture of the LSCs as French windows in a house. (b) The architecture and the operational mechanism of the LSCs. (c) A waveguide containing the luminescent conjugated polymer in this study, showing an intensive red-light edge emission.

perovskite nanocrystals.[33–35] Compared with these categories of luminophores that have been extensively studied, conjugated polymers are rarely reported for LSCs.[36–38] Gutierrez *et al*. reported two poly(arylene-*alt*-ethynylene)s, which were used with a perylene dicarboximide dye to form a donor–acceptor energy transfer system in thin-film LSCs.[36] Meazzini *et al*. reported a poly(fluorene-*alt*-phenylene) which was embedded in waveguides made of ureasil organic–inorganic hybrids for flexible LSCs.[37] Lyu *et al*. reported a poly(tetraphenylethylene), a green-emitting conjugated polymer with aggregation-induced emission properties, which was used as a donor in an energy transfer system to a red-emitting perylene acceptor.[38] Despite the few reports for LSCs, there are a tremendous number of reports on conjugated polymers for organic electronics. Conjugated polymers have been widely employed in organic PVs,[39–41] organic field-effect transistors,[42–44] organic thermoelectrics[45–47] etc., attributed to their unique optical, electronic and mechanical properties.[48–51]

To extend the study of conjugated polymers for LSCs, in this report we introduce a conjugated polymer with a photoluminescence quantum yield (PLQY) of 0.40, which is relatively high compared with other conjugated polymers, and we investigate the performance of LSCs based on this luminescent conjugated polymer. As demonstrated in Fig. 1(c), the waveguide containing the luminescent conjugated polymer exhibited intense red-light edge emission. The LSCs, with a size of 12 in. (929.0304 cm^2), exhibited high power conversion efficiencies (PCEs) of 2.9% and 3.6% under outdoor direct sunlight and indoor diffuse light-emitting diode (LED) light, respectively.

EXPERIMENTAL

Materials and instrumentation

All chemicals were used as received without further purification. The conjugated polymer poly(naphthalene-*alt*-vinylene) (PNV) was synthesized according to the literature.[52] The chemical structure of PNV was confirmed by ^{1}H NMR, as shown in Fig. S1. It is a red-emitting polymer with high photostability.[52] It exhibits a number-average molecular weight (M_n) of 30 000 g mol^{-1} and a dispersity ($Đ$) of 2.3, which were characterized by gel permeation chromatography using tetrahydrofuran as eluent, as shown in Fig. S2. Poly(methyl methacrylate) (PMMA) (average $M_w \approx$ 15 000 g mol^{-1}) and anhydrous toluene were purchased from Sigma-Aldrich (St. Louis, MO, USA). Clear acrylic sheets with a thickness of 0.125 in. (0.3175 cm) were purchased from Home Depot (Atlanta, GA, USA). The liquid optically clear adhesive, which was used as a reagent to glue the components in the LSCs, was purchased from 3M (Saint Paul, MN, USA). Gallium arsenide (GaAs) solar cells were fabricated using a molecular beam epitaxy system according to the literature.[53] The dimensions of the GaAs solar cells were 1–12 in. (2.54–30.48 cm) long and 0.25 in. (0.635 cm) wide, which exactly matched the dimensions of the edge of the waveguide.

The absorption and emission spectra of PNV in the waveguide was measured using a Varian Cary 5000 UV–visible–NIR spectrometer and an ISS PC1 photon-counting spectrofluorometer, respectively. The PLQY of PNV was measured using an integrating sphere connected to a Hamamatsu C9920-12 external quantum efficiency (EQE) measurement system.

The experimental setup for measuring the PV performance of the solar cells and the LSCs under outdoor direct sunlight (1000 W $m^{-2} \pm 10\%$) and indoor diffuse LED light (10 W $m^{-2} \pm 10\%$) was according to the literature.[16] The measurements under outdoor direct sunlight were done in summer within a week to ensure that the terrestrial solar radiation did not vary a lot. The sunlight was from a clear sky, and its power density was monitored during the measurements. The AM1.5G solar spectrum is shown in Fig. S3. The measurements under outdoor direct sunlight reported the performance of the LSCs during a particular period. Although the solar irradiance varied in a year, the spectral mismatch factor was not considered in this study.[54] For the indoor diffuse LED light, the CIE 1931 *xy* coordinates were (0.45, 0.42), which is depicted in Fig. S3. The corresponding correlated color temperature (McCamy's approximation) was 2884 K. In this report, we present the *J*–*V* curves instead of the *I*–*V* curves of the LSCs because the *J*–*V* curves directly indicated the PV performance of the LSCs without knowing the LSC size.[55] The *J*–*V* curves of the solar cells and the LSCs were measured with a Keithley 2401 source meter. The averaged PV parameters and the standard errors from the *J*–*V* curves of the LSCs are listed in Tables S1–S4. For a clear presentation of the results, the average values of the PV parameters are shown in this report. The EQE of the GaAs solar cells was measured on an Enlitech QE-R3011 system. The EQEs of the LSCs were measured according to standard protocols for common PV devices. The entire front surface was illuminated by a large-area (50 × 50 cm^2) monochromatic incident light, and the corresponding short-circuit current was measured. The power of the monochromatic incident light was measured using a reference solar cell with known EQE.[56]

Fabrication of the LSCs

The architecture of the LSCs in this study consisted of a thin layer of PNV-doped PMMA sandwiched between two clear acrylic

sheets. The preparation of a thin layer of PNV-doped PMMA was according to the literature.[57–59] The detailed procedures for the fabrication of the LSCs are shown in Fig. 2. To begin with, PMMA powder was dissolved in toluene, and the mixture was stirred overnight followed by the removal of insoluble residues through filtration and the addition of PNV (1 wt% relative to the amount of PMMA in toluene) according to the literature.[57–59] This doping concentration allowed PNV in the LSCs to exhibit an absorbance of 4.0 and therefore to absorb 99.99% of the incident light at the absorption wavelength of PNV. Then, the mixture was poured onto a clear acrylic sheet in a home-made stainless-steel mold. A thin layer of PNV-doped PMMA (approximately 15 μm) was obtained after removal of the solvent through slow evaporation under ambient conditions. Finally, a liquid optically clear adhesive for index matching was applied to the thin layer, and another clear acrylic sheet was placed on the top of the thin layer. The raw sandwich-type luminescent waveguide was placed in an oven at 100 °C for 2 h to cure the liquid optically clear adhesive. After removal of the mold, the raw luminescent waveguide was cut and polished by power tools into a square from 1 in. (2.54 cm) to 12 in. (30.48 cm). The final thickness of the luminescent waveguide was 0.25 in. (0.635 cm). The solar cells were attached to all four edges of the luminescent waveguide using the liquid optically clear adhesive for index matching. They were connected in parallel to maximize the device performance.[60]

RESULTS AND DISCUSSION

Properties of PNV and the GaAs solar cells

First, we show and discuss the spectroscopic properties of PNV and the PV properties of the GaAs solar cells. As shown in Fig. 3(a), PNV is a conjugated polymer with vinylene-bridged naphthalene diimide (NDI) as the backbone repeating unit. Its absorption (λ_{abs}) and emission (λ_{em}) wavelengths, measured in the PMMA matrix, are 535 and 632 nm, respectively. Its PLQY in PMMA is 0.40, which is higher than the solid-state PLQY previously reported in the literature (PLQY = 0.33).[52] This possibly indicates that PMMA is a good host matrix to reduce the non-radiative decay loss in the emission process of PNV. Studies have shown that intermolecular interactions and aggregation between polymer chains are inhibited in the PMMA matrix, which decreases photoluminescence quenching.[61,62] Figure 3(b) presents the absorption and emission spectra of PNV in PMMA. The absorption peak at 535 nm is ascribed to the intramolecular charge transfer (ICT) transition between the NDI unit and the vinylene unit, while the absorption peak at 332 nm is ascribed to the local excited state.[63–65] Due to the ICT characteristic, PNV exhibits a large Stokes shift of 97 nm with a long-wavelength emission centered at 632 nm. The self-absorption cross-section per 1 cm optical path (σ_{SA}) of PNV, calculated from the spectral overlap, is only 4.9%, which suggests that the PNV-based LSCs will show a slow decrease in performance with increasing size.[66] Due to the wide absorption range of PNV, the PNV-based LSCs will be capable of absorbing 43% AM1.5G solar photons and 62% LED photons in the spectral range between 300 and 900 nm, which is depicted in Figs 3(c) and 3(d), respectively. This signifies that the LSCs will exhibit high performance in these light conditions. The absolute absorption and transmission spectra of PNV in the LSCs are provided in Fig. S4. In the measurements of the absolute absorption and transmission spectra of PNV in the LSCs, the absorption and transmission spectra of blank LSCs were subtracted from those of the PNV-based LSCs. The reflection was canceled out.

The GaAs solar cells in this study had a stack architecture as shown in Fig. 3(e). The layers contained p-type and n-type GaAs, p-type $GaInP_2$ and n-type $AlInP_2$. A layer 3200 nm thick of p-type GaAs was the major light-absorbing layer. Figures 3(f), 3(g) depict the *J–V* curves of the GaAs solar cells measured under outdoor direct sunlight and indoor diffuse LED light, respectively. Under outdoor direct sunlight (1000 W m^{-2} ± 10%), the GaAs solar cells exhibited, on average, a short-circuit current density (J_{sc}) of 278 A m^{-2}, an open-circuit voltage (V_{oc}) of 1.03 V and a fill factor (FF) of 0.80. The corresponding PCE (η_{cell}) was 23.0%. Under indoor diffuse LED light (10 W m^{-2} ± 10%), the GaAs solar cells exhibited decreased performance, possibly due to the incapability of responding to the diffuse light. The J_{sc}, V_{oc} and FF dropped to 2.08 A m^{-2}, 0.79 V and 0.76, respectively, and the corresponding η_{cell} decreased to 12.4%. The EQE of the GaAs solar cells was also measured, which is shown in Fig. 3(h). The EQE was close to 0.9 between 550 and 850 nm, which matched the range of the emission spectrum of PNV and therefore was beneficial to maximize the performance of the PNV-based LSCs.

Performance of the LSCs

Next, we show and discuss the performance of the PNV-based LSCs. The size of the LSCs (*L*) was from 1 in. (2.54 cm) to 12 in. (30.48 cm), corresponding to a front surface area from 1 in^2

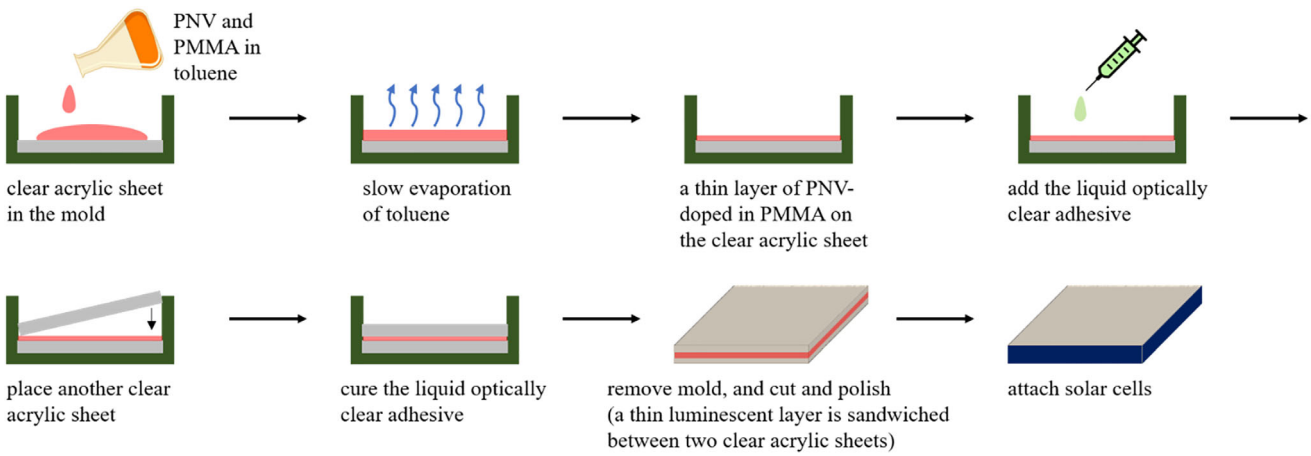

Figure 2. Fabrication procedures of the LSCs.

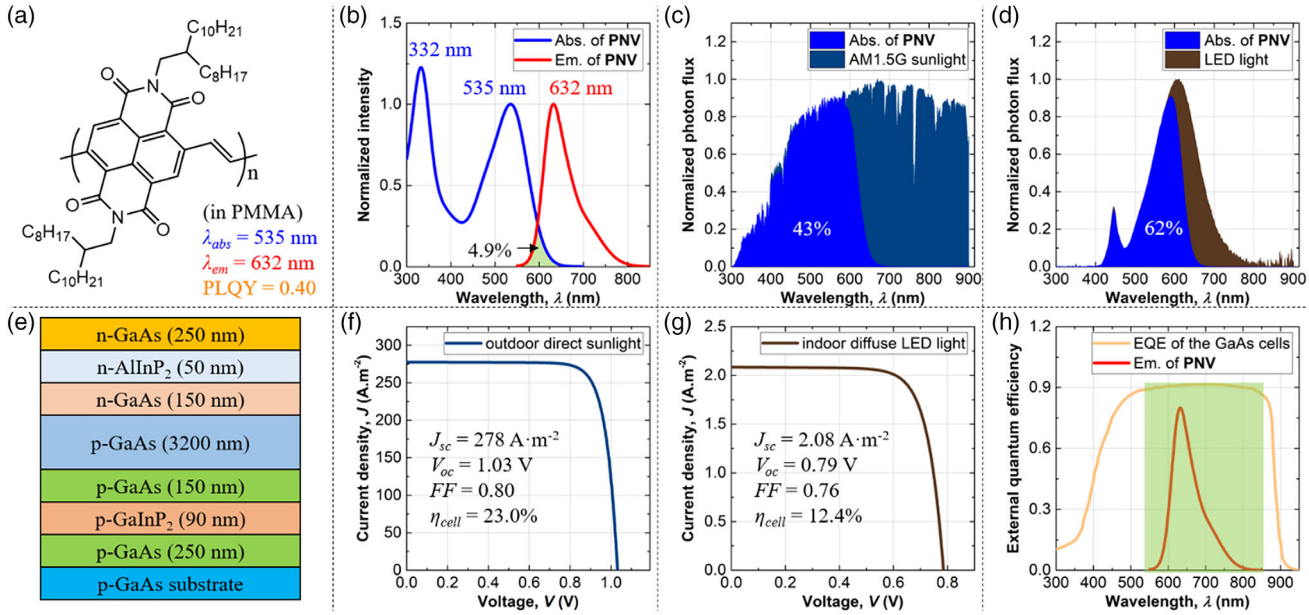

Figure 3. (a) Structure and spectroscopic properties of PNV. (b) Normalized absorption and emission spectra of PNV. Absorption percentage of the LSCs under (c) AM1.5G sunlight and (d) LED light. (e) Stack architecture of the GaAs solar cells. *J–V* curves and PV parameters of the GaAs solar cells measured under (f) outdoor direct sunlight and (g) indoor diffuse LED light. (h) EQE of the GaAs solar cells superimposed with the emission spectrum of PNV.

(6.4516 cm^2) to 144 in^2 (929.0304 cm^2). The *J–V* curves of the LSCs were measured under outdoor direct sunlight (1000 W m^{-2} ± 10%) and indoor diffuse LED light (10 W m^{-2} ± 10%). The performance of the LSCs before and after a surface scattering treatment (SST) was investigated. The purpose of the SST was to introduce proper light scattering by roughening the waveguide surface to boost the performance and the cost-effectiveness of the LSCs. The surface root-mean-squared roughness (R_q) was 63 nm, measured by AFM, for the LSCs after the SST. The detailed procedures for the SST are described in the literature.[67] The performance of the LSC is described using two parameters.[68] The first parameter is the PCE of the LSC (η_{LSC}), which is the output power of the LSC (P_{LSC}) relative to the input power of the incident light (P_{in}). Unlike other studies that reported the optical efficiency of the luminescent waveguide (η_{opt}),[69–71] this study reports η_{LSC} because it is practically relevant and directly reflects the PV performance of the LSC. The second parameter is the concentration ratio (*C*) of the LSC. It is the P_{LSC} relative to the output power of the solar cells (P_{cell}) when the solar cells are detached from the luminescent waveguide measured under the same incident light. The higher the *C* is, the more cost-effective is the LSC. η_{LSC} and *C* are obtained from the *J–V* curve of the LSC using

$$\eta_{LSC} = \frac{P_{LSC}}{P_{in}} = A_{front} \times \frac{J_{sc} V_{oc} FF}{P_{in}} \quad (1)$$

$$C = \frac{P_{LSC}}{P_{cell}} = \frac{A_{front}}{A_{edge}} \times \frac{J_{sc} V_{oc} FF}{J_{sc,cell} V_{oc,cell} FF_{cell}} \quad (2)$$

where A_{front} and A_{edge} are the areas of the front surface and the edge of the waveguide, respectively. The expression P_{in}/A_{front} is the incident power density, which is 1000 W m^{-2} ± 10% for outdoor direct sunlight and 10 W m^{-2} ± 10% for indoor diffuse LED light. It should be emphasized that only A_{front} should be applied to calculate η_{LSC}.

Figures 4(a) and 4(b) show the *J–V* curves of the LSCs under outdoor direct sunlight. The results demonstrate that the LSCs exhibit a significantly improved J_{sc} from below 30 A m^{-2} before the SST to over 30 A m^{-2} after the SST. Also, J_{sc} decreased with increasing *L*. The effect of the SST on the performance of the LSCs is more evident in Figs 4(c) and 4(d). The LSCs after the SST exhibited significantly higher η_{LSC} and *C* than those before the SST. For example, the η_{LSC} and the *C* of the 6-in. (232.2576 cm^2) LSC were improved from 1.5% to 3.4% and from 0.38 to 0.88, respectively, after the SST. Despite the overall increase of η_{LSC} and *C*, the LSCs after the SST exhibited a faster decrease of η_{LSC} and a slower increase of *C* with increasing *L*. For example, with *L* increasing from 1 in. (2.54 cm) to 12 in. (30.48 cm), η_{LSC} decreased from 4.9% to 2.9% (by −41%) and *C* increased from 0.21 to 1.49 (by +610%) for the LSCs after the SST. The LSCs before the SST exhibited a relatively slow decrease of η_{LSC} from 2.0% to 1.3% (by −35%) and a relatively fast increase of *C* from 0.09 to 0.67 (by +644%). The results indicated that the scattering effect brought by the SST was very sensitive to the device size because the photon scattering effect inside the luminescent waveguide led to performance gain and loss. With *L* increased beyond 12 in. (30.48 cm), there would be a certain point where the SST becomes ineffective, suggestive of the balance between the performance gain and loss.

The performance of the LSCs under indoor diffuse LED light was quite different from that under outdoor direct sunlight. As shown in Figs 4(e) and 4(f), the LSCs exhibited J_{sc} between 0.4 A m^{-2} and 1.2 A m^{-2}, suggestive of the ineffectiveness of the SST. Figures 4 (g) and 4(h) demonstrated more direct results, showing that the SST harmed the performance of the LSCs. For example, η_{LSC} and *C* were reduced from 4.7% to 3.7% and from 2.27 to 1.81, respectively, for the 6-in. (232.2576 cm^2) LSC after SST. Associated with a fast decrease of η_{LSC} and a slow increase of *C* with increasing *L*, the adverse effect of the SST on the performance of the LSCs became more apparent. For example, with *L* increased from 1 in. (2.54 cm) to 12 in. (30.48 cm), η_{LSC} decreased from 5.7% to 2.7% (by −53%) and *C* increased from 0.46 to 2.66 (by +482%) for the LSCs after the SST. The LSCs before the SST exhibited a relatively slower decrease of η_{LSC} from 6.1% to 3.6% (by −41%) and a relatively fast increase of *C* from 0.49 to 3.53 (by 620%). The results signified that

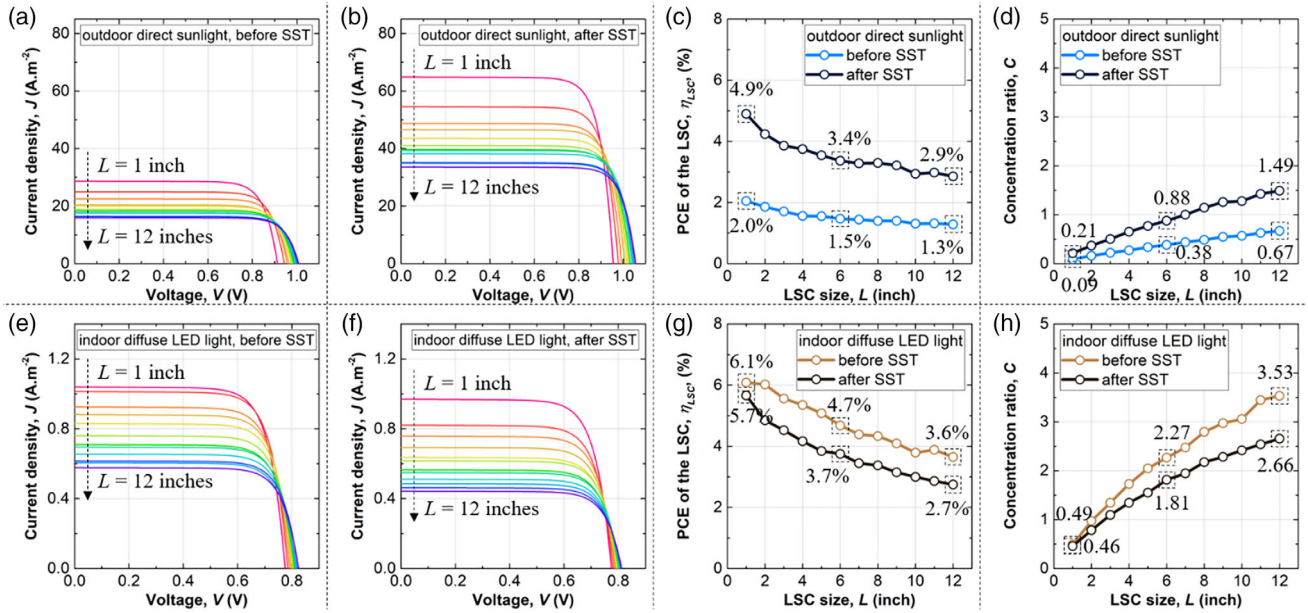

Figure 4. *J–V* curves of the LSCs measured under outdoor direct sunlight (a) before and (b) after the SST. (c) η_{LSC} and (d) *C* measured under outdoor direct sunlight. *J–V* curves of the LSCs measured under indoor diffuse LED light (e) before and (f) after the SST. (g) η_{LSC} and (h) *C* measured under indoor diffuse LED light.

the SST was not suitable for the LSCs that were used under the indoor diffuse LED light, which has not been revealed previously. This was because the diffuse incident light provides an effect very similar to the scattering effect, and therefore the SST on the LSCs under indoor diffuse LED light was not helpful, while it further disturbed the photon transport inside the luminescent waveguide, causing the performance reduction.

We also measured the performance of the blank (i.e. without PNV) LSCs with increasing *L* before and after the SST to understand the role of the scattering effect in the waveguide, which is shown in Tables S5–S8. Before the SST, η_{LSC} varied around 1.13% and 3.76% for the LSCs measured under outdoor direct sunlight and indoor diffuse LED light, respectively. After the SST, η_{LSC} decreased from 2.36% to 1.75% and from 3.33% to 2.84% with *L* increasing from 1 in. (2.54 cm) to 12 in. (30.48 cm) for the LSCs measured under outdoor direct sunlight and indoor diffuse LED light, respectively. These results suggest that the contribution of the performance of the LSCs from the scattering effect was comparable to that from the luminescence. The performance of the blank LSCs was attributed to the slightly rough surface of the waveguide during fabrication, which has been investigated in our previous study.[67] The LSCs after the SST could be considered as hybrid luminescent/scattering solar concentrators.

The results from the performance of the PNV-based LSCs suggest that the LSCs performed more efficiently under indoor diffuse LED light than outdoor direct sunlight. The LSC with the largest area (i.e. 929.0304 cm^2) in this study exhibited an η_{LSC} of 2.9% and a *C* of 1.49 under outdoor direct sunlight after the SST and exhibited an η_{LSC} of 3.6% and a *C* of 3.53 under indoor diffuse LED light before the SST. As shown in Table S9 the PNV-based LSCs were among the high-performance large-area LSCs.[72–78]

Analysis of the LSCs

Information on the EQEs of the LSCs and the edge emission spectra of the luminescent waveguides helped us to get a deeper understanding of the device performance. Here, as a representative example, we presented the EQEs of a 6-in. (232.2576 cm^2) LSC and the edge emission spectra of the corresponding luminescent waveguide before and after SST under outdoor direct sunlight and indoor diffuse LED light. The EQEs of the LSCs were generally measured under direct incident light. Therefore, the results only reflected the device performance under direct incident light, which in this study was the outdoor direct sunlight. As shown in Fig. 5(a), there was a significant difference between the EQEs of the LSCs before and after the SST. For the LSC before the SST, the EQE before 640 nm was higher than that after 640 nm. Since 640 nm was close to the absorption onset of PNV (see Fig. 3(b)), the results suggest that the device performance primarily came from the TIR-based photon transport, and a large fraction of the TIR-based photons was from the luminophore emission while a small fraction was due to the scattering effect of the luminescent waveguide, which was evidenced in the results that a relatively low EQE was obtained after 640 nm. The scattering effect at the long-wavelength range was common for the LSCs because of the imperfect surface smoothness of the waveguide and the host matrix scattering. This has been observed in reports where standard protocols were used to measure the EQEs of the LSCs.[6,60,79–81] For the LSC after the SST, the scattering effect dominated the device performance, and a significantly high EQE was obtained after 640 nm. Before 640 nm, the LSC exhibited a relatively low EQE, which indicated that the SST affected the TIR-based photon transport, especially for photons from the luminophore emission. The high performance of the LSCs after the SST under outdoor direct sunlight came from the combined effects of the luminophore emission and the surface scattering (see Tables S1–S8). This was also confirmed by the EQE of the blank LSC before the SST, which is shown in Fig. S5. The EQE of the blank LSC was comparable to that of the PNV-based LSC before the SST. Integrating the EQEs with AM1.5G sunlight afforded J_{sc} of 19.0 and 41.8 A m^{-2} for the 6-in. (232.2576 cm^2) LSC under outdoor direct sunlight before and after the SST, respectively, which are consistent with the J_{sc} from the *J–V* curves in Figs 4(a) and 4(b), respectively.

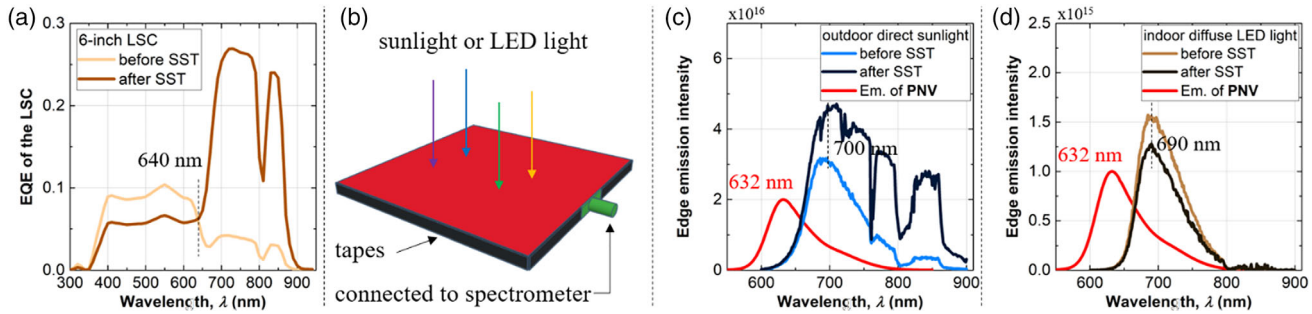

Figure 5. (a) The EQE of the 6-in. (232.2576 cm^2) LSC before and after the SST. (b) The experimental setup to measure the edge emission spectrum of the 6-in. (232.2576 cm^2) luminescent waveguide. Edge emission spectra of the luminescent waveguides before and after the SST under (c) outdoor direct sunlight and (d) indoor diffuse LED light superimposed with the emission spectrum of PNV.

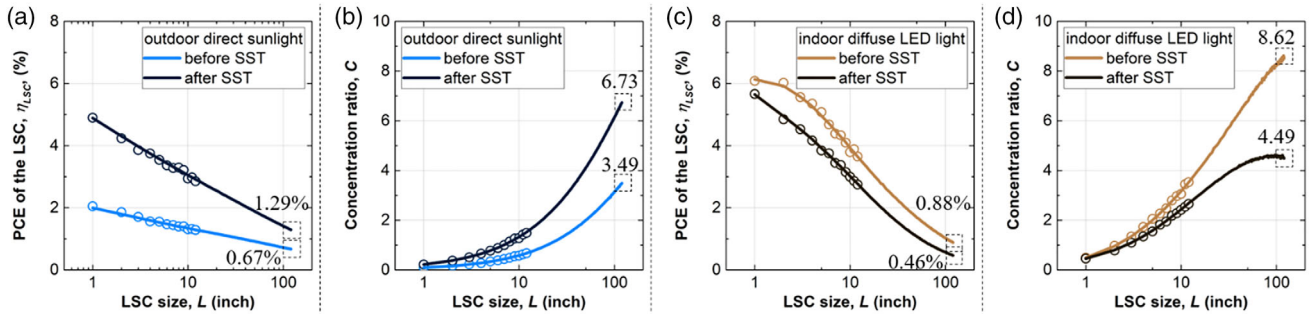

Figure 6. The projected (a) η_{LSC} and (b) C for the LSCs under outdoor direct sunlight. The projected (c) η_{LSC} and (d) C for the LSCs under indoor diffuse LED light.

Figure 5(b) shows the experimental setup to measure the edge emission spectrum of the 6-in. (232.2576 cm^2) luminescent waveguide. The waveguide edge was covered with blackout tapes except for the area that was connected to the spectrometer. As depicted in Fig. 5(c), under outdoor direct sunlight the luminescent waveguide exhibited a higher edge emission intensity after the SST, and the edge emission after 700 nm was primarily from the scattering effect due to the SST. This was confirmed when this observation was compared with the edge emission spectrum of the blank waveguide before the SST, which is shown in Fig. S6. The edge emission of the luminescent waveguide under outdoor direct sunlight, despite the SST, maximized around 700 nm, which was 68 nm greater than the emission wavelength of PNV (632 nm), suggestive of luminophore self-absorption that red-shifted the emission combined with the scattered outdoor direct sunlight. For the luminescent waveguide under indoor diffuse LED light, the edge emission intensity decreased after the SST as depicted in Fig. 5(d). The edge emission, despite the SST, exhibited a maximum of around 690 nm, which was a red-shift of 58 nm compared with the emission wavelength of PNV (632 nm). Compared with the red-shift (68 nm) for the luminescent waveguide under outdoor direct sunlight, the smaller red-shift (58 nm) for the luminescent waveguide under indoor diffuse LED light signified the absence of near-infrared photons in the indoor diffuse LED light. We also applied regional measurements to the 6-in. (232.2576 cm^2) LSC before and after the SST under a monochromatic incident light of 540 nm. The results are shown in Fig. S7. The results suggest that the SST decreased the photon transport efficiency for visible photons, which is consistent with the results in Fig. 5(a).

Projected performance of the LSCs

Our final task was to investigate the performance of large-area (> 1000 cm^2) LSCs. To this end, we performed Monte Carlo ray-tracing simulations to project the device performance.[82–84] Typical loss mechanisms were considered in the simulation, which were incomplete absorption of the incident light, luminophore self-absorption, matrix absorption, internal scattering and surface scattering. Wavelength-dependent parameters were used in the simulation for describing the loss mechanisms.[8] The size of the LSCs was from 1 in. (2.54 cm) to 120 in. (304.8 cm). As shown in Fig. 6, the simulated results (solid lines) in the range L = 1–12 in. (2.54–30.48 cm) were consistent with the experimental results (dotted data). For the LSCs under outdoor direct sunlight, with increasing L the projected η_{LSC} decreased (see Fig. 6(a)) while the projected C increased (see Fig. 6(b)). For the 120-in. (92 903.04 cm^2) LSCs before and after the SST, the projected η_{LSC} was 0.67% and 1.29%, respectively (see Fig. 6(a)), and the projected C was 3.49 and 6.73, respectively (see Fig. 6(b)). For the 120-in. (92 903.04 cm^2) LSCs before and after the SST under indoor diffuse LED light, the projected η_{LSC} was 0.46% and 0.88%, respectively (see Fig. 6(c)), and the projected C was 4.49 and 8.62, respectively (see Fig. 6(d)). The projected performance of the LSCs confirmed that the SST worked better for LSCs under outdoor direct sunlight than indoor diffuse LED light. For the 120-in. (92 903.04 cm^2) LSCs, although they exhibited low η_{LSC}, they exhibited high C. This indicated that the power output of the solar cells was significantly enhanced when the solar cells were attached to the luminescent waveguide, and therefore it indicated improved cost-effectiveness.

CONCLUSIONS

In this report, we investigated the performance of LSCs based on a luminescent conjugated polymer, PNV. In a PMMA matrix, PNV exhibited an absorption wavelength of 535 nm, which covered 43% and 62% of the photon spectrum of the sunlight and the LED light, respectively. Its emission wavelength was 632 nm, matching well with the EQE of the GaAs solar cells. PNV had a moderate PLQY of 0.40. The performance of the PNV-based LSCs with sizes of 1–12 in. (2.54–30.48 cm) was investigated under outdoor direct sunlight (1000 W m^{-2} ± 10%) and indoor diffuse LED light (10 W m^{-2} ± 10%) before and after the SST. The results showed that the 12-in. (929.03 cm^2) LSCs exhibited a high η_{LSC} of up to 2.9% and *C* of up to 1.49 when tested under outdoor direct sunlight after the SST, and they exhibited a high η_{LSC} of up to 3.6% and *C* of up to 3.53 when tested under indoor diffuse LED light before the SST. The EQE and the edge emission analysis on the 6-in. (232.06 cm^2) LSCs showed that the SST significantly improved the EQE after 640 nm and the edge emission after 700 nm, especially under outdoor direct sunlight. Monte Carlo ray-tracing simulation was performed to project the performance of large-area LSCs with sizes of up to 120 in. (304.8 cm). The results showed that for the LSCs tested under outdoor direct sunlight and indoor diffuse LED light, with increasing *L* of up to 120 in. (304.8 cm) η_{LSC} decreased to 1.29% and 0.88%, respectively, and *C* increased to 6.73 and 8.62, respectively. This report suggests that the luminescent conjugated polymer PNV is a promising material for high-performance LSCs.

ACKNOWLEDGEMENTS

This work is a part of the project Energy-Harvesting Windows and Panels. The authors would like to thank Solera City Energy for research support.

CONFLICTS OF INTEREST

There are no conflicts of interest to declare.

SUPPORTING INFORMATION

Supporting information may be found in the online version of this article.

REFERENCES

1 Chemisana D, *Renewable Sustainable Energy Rev* **15**:603–611 (2011). https://doi.org/10.1016/j.rser.2010.07.017.
2 Norton B, Eames PC, Mallick TK, Huang MJ, McCormack SJ, Mondol JD *et al.*, *Sol Energy* **85**:1629–1664 (2011). https://doi.org/10.1016/j.solener.2009.10.004.
3 Jelle BP, Breivik C and Røkenes HD, *Sol Energy Mater Sol Cells* **100**:69–96 (2012). https://doi.org/10.1016/j.solmat.2011.12.016.
4 Shukla AK, Sudhakar K and Baredar P, *Energy Buildings* **128**:99–110 (2016). https://doi.org/10.1016/j.enbuild.2016.06.077.
5 Yang T and Athienitis AK, *Renewable Sustainable Energy Rev* **66**:886–912 (2016). https://doi.org/10.1016/j.rser.2016.07.011.
6 van Sark WG, Barnham KW, Slooff LH, Chatten AJ, Buchtemann A, Meyer A *et al.*, *Opt Express* **16**:21773–21792 (2008). https://doi.org/10.1364/oe.16.021773.
7 Scudo PF, Abbondanza L, Fusco R and Caccianotti L, *Sol Energy Mater Sol Cells* **94**:1241–1246 (2010). https://doi.org/10.1016/j.solmat.2010.03.015.
8 Debije MG and Verbunt PPC, *Adv Energy Mater* **2**:12–35 (2012). https://doi.org/10.1002/aenm.201100554.
9 Meinardi F, Bruni F and Brovelli S, *Nat Rev Mater* **2**:17072 (2017). https://doi.org/10.1038/natrevmats.2017.72.
10 Reinders A, Kishore R, Slooff L, Eggink W and Jpn J, *Appl Phys* **57**:08RD10 (2018). https://doi.org/10.7567/JJAP.57.08RD10.
11 McKenna B and Evans RC, *Adv Mater* **29**:1606491 (2017). https://doi.org/10.1002/adma.201606491.
12 Desmet L, Ras AJ, de Boer DK and Debije MG, *Opt Lett* **37**:3087–3089 (2012). https://doi.org/10.1364/ol.37.003087.
13 Mouedden YE, Ding B, Song Q, Li G, Nguyen H and Alameh K, *J Appl Phys* **118**:015502 (2015). https://doi.org/10.1063/1.4923389.
14 Li Y, Olsen J, Nunez-Ortega K and Dong W-J, *Sol Energy* **136**:668–674 (2016). https://doi.org/10.1016/j.solener.2016.07.051.
15 Debije MG and Rajkumar VA, *Sol Energy* **122**:334–340 (2015). https://doi.org/10.1016/j.solener.2015.08.036.
16 Li Y, Sun Y and Zhang Y, *Sol Energy* **188**:1248–1255 (2019). https://doi.org/10.1016/j.solener.2019.07.035.
17 Weber WH and Lambe J, *Appl Optics* **15**:2299–2300 (1976). https://doi.org/10.1364/ao.15.002299.
18 Goetzberger A and Greube W, *Appl Phys* **14**:123–139 (1977). https://doi.org/10.1007/bf00883080.
19 Sanguineti A, Sassi M, Turrisi R, Ruffo R, Vaccaro G, Meinardi F *et al.*, *Chem Commun* **49**:1618–1620 (2013). https://doi.org/10.1039/c2cc38708e.
20 Benjamin WE, Veit DR, Perkins MJ, Bain E, Scharnhorst K, McDowall S *et al.*, *Chem Mater* **26**:1291–1293 (2014). https://doi.org/10.1021/cm403286v.
21 Mateen F, Lee SY and Hong S-K, *J Mater Chem A* **8**:3708–3716 (2020). https://doi.org/10.1039/C9TA13312G.
22 Banal JL, Zhang B, Jones DJ, Ghiggino KP and Wong WW, *Acc Chem Res* **50**:49–57 (2017). https://doi.org/10.1021/acs.accounts.6b00432.
23 Zhang B, Banal JL, Jones DJ and Tang BZ, *Mater Chem Front* **2**:615–619 (2018). https://doi.org/10.1039/C7QM00598A.
24 Pucci A, *Isr J Chem* **58**:837–844 (2018). https://doi.org/10.1002/ijch.201800028.
25 Purcell-Milton F and Gun'ko YK, *J Mater Chem* **22**:16687–16697 (2012). https://doi.org/10.1039/c2jm32366d.
26 Zhou Y, Zhao H, Ma D and Rosei F, *Chem Soc Rev* **47**:5866–5890 (2018). https://doi.org/10.1039/c7cs00701a.
27 Li Z, Zhao X, Huang C and Gong X, *J Mater Chem C* **7**:12373–12387 (2019). https://doi.org/10.1039/C9TC03520F.
28 Ma Y, Zhang Y and Yu WW, *J Mater Chem C* **7**:13662–13679 (2019). https://doi.org/10.1039/C9TC04065J.
29 Liu C, Deng R, Gong Y, Zou C, Liu Y, Zhou X *et al.*, *Int J Photoenergy* **2014**:290952 (2014). https://doi.org/10.1155/2014/290952.
30 Freitas VT, Fu L, Cojocariu AM, Cattoën X, Bartlett JR, Parc RL *et al.*, *ACS Appl Mater Interfaces* **7**:8770–8778 (2015). https://doi.org/10.1021/acsami.5b01281.
31 Frias AR, Cardoso MA, Bastos ARN, Correia SFH, André PS, Carlos LD *et al.*, *Energies* **12**:451 (2019). https://doi.org/10.3390/en12030451.
32 Correia SFH, VdZ B, SJL R, André PS, RAS F and Carlos LD, *J Mater Chem A* **2**:5580–5596 (2014). https://doi.org/10.1039/C3TA14964A.
33 Cohen TA, Milstein TJ, Kroupa DM, MacKenzie JD, Luscombe CK and Gamelin DR, *J Mater Chem A* **7**:9279–9288 (2019). https://doi.org/10.1039/C9TA01261C.
34 Zhao H, Sun R, Wang Z, Fu K, Hu X and Zhang Y, *Adv Funct Mater* **29**:1902262 (2019). https://doi.org/10.1002/adfm.201902262.
35 Li Z, Johnston A, Wei M, Saidaminov MI, JMd P, Zheng X *et al.*, *Joule* **4**:631–643 (2020). https://doi.org/10.1016/j.joule.2020.01.003.
36 Gutierrez GD, Coropceanu I, Bawendi MG and Swager TM, *Adv Mater* **28**:497–501 (2016). https://doi.org/10.1002/adma.201504358.
37 Meazzini I, Blayo C, Arlt J, Marques A-T, Scherf U, Burrows HD *et al.*, *Mater Chem Front* **1**:2271–2282 (2017). https://doi.org/10.1039/C7QM00264E.
38 Lyu G, Kendall J, Meazzini I, Preis E, Baysec S, Scherf U *et al.*, *ACS Appl Polym Mater* **1**:3039–3047 (2019). https://doi.org/10.1021/acsapm.9b00718.
39 Su Y-W, Lan S-C and Wei K-H, *Mater Today* **15**:554–562 (2012). https://doi.org/10.1016/S1369-7021(13)70013-0.
40 Holliday S, Li Y and Luscombe CK, *Prog Polym Sci* **70**:34–51 (2017). https://doi.org/10.1016/j.progpolymsci.2017.03.003.
41 Inganas O, *Adv Mater* **30**:1800388 (2018). https://doi.org/10.1002/adma.201800388.
42 Katz HE and Bao Z, *J Phys Chem B* **104**:671–678 (2000). https://doi.org/10.1021/jp992853n.

43 Allard S, Forster M, Souharce B, Thiem H and Scherf U, *Angew Chem Int Ed* **47**:4070–4098 (2008). https://doi.org/10.1002/anie.200701920.
44 Braga D and Horowitz G, *Adv Mater* **21**:1473–1486 (2009). https://doi.org/10.1002/adma.200802733.
45 Zhang Q, Sun Y, Xu W and Zhu D, *Adv Mater* **26**:6829–6851 (2014). https://doi.org/10.1002/adma.201305371.
46 Chen Y, Zhao Y and Liang Z, *Energ Environ Sci* **8**:401–422 (2015). https://doi.org/10.1039/C4EE03297G.
47 Russ B, Glaudell A, Urban JJ, Chabinyc ML and Segalman RA, *Nat Rev Mater* **1**:16050 (2016). https://doi.org/10.1038/natrevmats.2016.50.
48 Li Y, Tatum WK, Onorato JW, Barajas SD, Yang YY and Luscombe CK, *Polym Chem* **8**:5185–5193 (2017). https://doi.org/10.1039/C7PY00435D.
49 Li Y, Tatum WK, Onorato JW, Zhang Y and Luscombe CK, *Macromolecules* **51**:6352–6358 (2018). https://doi.org/10.1021/acs.macromol.8b00898.
50 Hu Z, Sun C, Lin A, Jackson J, Terlier T, Owolabi D *et al.*, *Adv Opt Mater* **8**:2000516 (2020). https://doi.org/10.1002/adom.202000516.
51 Sommerville PJW, Li Y, Dong BX, Zhang Y, Onorato JW, Tatum WK *et al.*, *Macromolecules* **53**:7511–7518 (2020). https://doi.org/10.1021/acs.macromol.0c00512.
52 Liang X, Tan L, Liu Z, Ma Y, Zhang G, Wang L *et al.*, *Chem Commun* **53**:4934–4937 (2017). https://doi.org/10.1039/c7cc01372h.
53 Lu S, Ji L, He W, Dai P, Yang H, Arimochi M *et al.*, *Nanoscale Res Lett* **6**:576 (2011). https://doi.org/10.1186/1556-276X-6-576.
54 Chantana J, Mano H, Horio Y, Hishikawa Y and Minemoto T, *Renewable Energy* **114**:567–563 (2017). https://doi.org/10.1016/j.renene.2017.07.061.
55 Li Y, Sun Y and Zhang Y, *Renewable Energy* **160**:127–135 (2020). https://doi.org/10.1016/j.renene.2020.06.121.
56 Li Y, Zhang Y, Sun Y and Ren T, *Appl Opt* **59**:8964–8969 (2020). https://doi.org/10.1364/AO.403354.
57 Li Y, Li Z, Wang Y, Compaan A, Ren T and Dong W-J, *Energy Environ Sci* **6**:2907–2911 (2013). https://doi.org/10.1039/C3EE42001A.
58 Li Y, Li Z, Ablekim T, Ren T and Dong WJ, *Phys Chem Chem Phys* **16**:26193–26202 (2014). https://doi.org/10.1039/c4cp03521f.
59 Li Y, Olsen J and Dong WJ, *Photochem Photobiol Sci* **14**:833–841 (2015). https://doi.org/10.1039/c4pp00480a.
60 Slooff LH, Bende EE, Burgers AR, Budel T, Pravettoni M, Kenny RP *et al.*, *Phys Status Solidi RRL* **2**:257–259 (2008). https://doi.org/10.1002/pssr.200802186.
61 Aharon E, Albo A, Kalina M and Frey GL, *Adv Funct Mater* **16**:980–986 (2006). https://doi.org/10.1002/adfm.200500458.
62 Rao KV, Jain A and George SJ, *J Mater Chem C* **2**:3055–3064 (2014). https://doi.org/10.1039/C3TC31729C.
63 Li Y, Scudiero L, Ren T and Dong W-J, *J Photochem Photobiol A* **231**:51–59 (2012). https://doi.org/10.1016/j.jphotochem.2012.01.011.
64 Kerner R, Li Y and Scudiero L, *Synth Met* **162**:1198–1203 (2012). https://doi.org/10.1016/j.synthmet.2012.04.010.
65 Li Y, Ren T and Dong W-J, *J Photochem Photobiol A* **251**:1–9 (2013). https://doi.org/10.1016/j.jphotochem.2012.10.002.
66 Krumer Z, Pera SJ, RJAv D-M, Zhao Y, AFPd B, Groeneveld E *et al.*, *Sol Energy Mater Sol Cells* **111**:57–65 (2013). https://doi.org/10.1016/j.solmat.2012.12.028.
67 Li Y, Sun Y and Zhang Y, *Sol Energy* **198**:151–159 (2020). https://doi.org/10.1016/j.solener.2020.01.038.
68 Li Y, Zhang X, Zhang Y, Dong R and Luscombe CK, *J Polym Sci A* **57**:201–215 (2019). https://doi.org/10.1002/pola.29192.
69 Mateen F, Ali M, Lee SY, Jeong SH, Ko MJ and Hong S-K, *Sol Energy* **190**:488–494 (2019). https://doi.org/10.1016/j.solener.2019.08.045.
70 Mateen F, Saeed MA, Shim JW and Hong S-K, *Sol Energy* **207**:379–387 (2020). https://doi.org/10.1016/j.solener.2020.06.104.
71 Mateen F, Li Y, Saeed MA, Sun Y, Zhang Y, Lee SY *et al.*, *J Lumin* **231**:117837 (2021). https://doi.org/10.1016/j.jlumin.2020.117837.
72 Meinardi F, Colombo A, Velizhanin KA, Simonutti R, Lorenzon M, Beverina L *et al.*, *Nat Photonics* **8**:392–399 (2014). https://doi.org/10.1038/nphoton.2014.54.
73 Meinardi F, McDaniel H, Carulli F, Colombo A, Velizhanin KA, Makarov NS *et al.*, *Nat Nanotechnol* **10**:878–885 (2015). https://doi.org/10.1038/nnano.2015.178.
74 Zhao H, Zhou Y, Benetti D, Ma D and Rosei F, *Nano Energy* **37**:214–223 (2017). https://doi.org/10.1016/j.nanoen.2017.05.030.
75 Wu K, Li H and Klimov VI, *Nat Photonics* **12**:105–110 (2018). https://doi.org/10.1038/s41566-017-0070-7.
76 Brennan LJ, Purcell-Milton F, McKenna B, Watson TM, Gun'ko YK and Evans RC, *J Mater Chem A* **6**:2671–2680 (2018). https://doi.org/10.1039/C7TA04731B.
77 Zhang B, Zhao P, Wilson LJ, Subbiah J, Yang H, Mulvaney P *et al.*, *ACS Energy Lett* **4**:1839–1844 (2019). https://doi.org/10.1021/acsenergylett.9b01224.
78 Roncali J, *Adv Energy Mater* **10**:2001907 (2020). https://doi.org/10.1002/aenm.202001907.
79 Bomm J, Büchtemann A, Chatten AJ, Bose R, Farrell DJ, Chan NLA *et al.*, *Sol Energy Mater Sol Cells* **95**:2087–2094 (2011). https://doi.org/10.1016/j.solmat.2011.02.027.
80 Pravettoni M, CSP L and Kenny RP, *Am J Eng Appl Sci* **9**:53–63 (2016). https://doi.org/10.3844/ajeassp.2016.53.63.
81 Li Y, Sun Y, Zhang Y and Dong W-J, *Opt Mater* **108**:110194 (2020). https://doi.org/10.1016/j.optmat.2020.110194.
82 Sahin D, Ilan B and Kelley DF, *J Appl Phys* **110**:033108 (2011). https://doi.org/10.1063/1.3619809.
83 Leow SW, Corrado C, Osborn M, Isaacson M, Alers G and Carter SA, *J Appl Phys* **113**:214510 (2013). https://doi.org/10.1063/1.4807413.
84 Shu JP, Zhang XW, Wang PJ, Chen RW, Zhang HH, Li DK *et al.*, *Phys B* **548**:53–57 (2018). https://doi.org/10.1016/j.physb.2018.08.021.

